Supporting Information

Tuning the active sites and optimizing the d-spacing value in CoFe-LDH by ex-situ intercalation of guest anions: an innovative electrocatalyst for overall water splitting reaction

*Sreenivasan Nagappan,[†‡] Arun Karmakar,[†‡] Ragunath Madhu,[†‡] Hariharan N Dhandapani,[†‡] Suprobhat Singha Roy,[†‡] and Subrata Kundu[†‡]**

[†]*Academy of Scientific and Innovative Research (AcSIR), Ghaziabad-201002, India.*

[‡]*Electrochemical Process Engineering (EPE) Division, CSIR-Central Electrochemical Research Institute (CECRI), Karaikudi-630003, Tamil Nadu, India.*

*To whom correspondence should be addressed, *E-mail:* skundu@cecri.res.in; kundu.subrata@gmail.com, Phone: (+ 91) 4565-241487.

This file contains 28 pages in which the details of reagents, methods of synthesis, electrochemical characterizations, electrochemical results, and characterizations like EDS spectrum of FESEM, HR-TEM images,

No. of Figures: 19

No. Tables: 2

Reagents and Instruments

Cobalt (II) chloride hexahydrate ($CoCl_2 \cdot 6H_2O$), Iron (III) chloride tetrahydrate ($FeCl_3 \cdot 4H_2O$), were purchased from Sigma-Aldrich. Sodium carbonate (Na_2CO_3) was purchased from Merck. The electrochemical workstation AURT-M204 has been used for the entire OER studies. A typical three electrode set-up with 1M KOH is used as an electrolyte for for OER experiments. Hg/HgO reference electrode was purchased from CH instruments and graphite rod counter electrode and Nickel Foam (NF) working electrode was purchased from Alfa-Aesar. DI water was used throughout the entire experimental analysis. For handling the chemicals and glassware's for the synthesis process as well as the application part, safety glove, lab coat and safety glass were mandatory and used accordingly. The as prepared powder materials were subjected to initial characterization XRD. XRD analysis was done with a scanning rate of 5° min^{-1} in the 2θ range 5-90° using a Bruker X-ray powder diffractometer (XRD) with Cu Kα radiation (λ = 0.154 nm). Then the catalysts were characterized with FE-SEM instrument (SUPRA 55VP Carl Zeiss) with a separate EDS detector connected to that instrument. Energy Dispersive X-ray Spectroscopy (EDS) analysis was done with the assistance of FESEM instrument X-ray photoelectron spectroscopic (XPS) analysis was performed using a Theta Probe AR-XPS system (Thermo Fisher Scientific, UK). HR-TEM, (Tecnai^{TM} G2 TF20) working at an accelerating voltage of 200 kV and by Talos F200-S with HAADF elemental mapping.

Calculation of d-spacing value: The d-spacing values of all catalysts were calculated by using following formulae,

$$d = n\lambda / 2dSin\theta \quad \text{(S6)}$$

Calculated area associated with the reduction of Co^{3+} to Co^{2+} of CoFe-LDH/I^-= 0.0012408 VA

Hence, the associated charge is = 0.0012408 VA / 0.15 Vs^{-1}

= 0.008272 C

Now, the number of electron transferred is 0.008272 **C** / 1.602 $\times 10^{-19}$

= 0.0051635 $\times 10^{19}$

Since, the reduction of Co^{3+} to Co^{2+} is a single electron transfer reaction, the number electron calculated above is exactly the same as the number of surface-active sites.

Hence, the number of Co participate in OER is = 5.1635 $\times 10^{16}$

Calculated area associated with the reduction of Co^{3+} to Co^{2+} of CoFe-LDH/Br^-= VA

Hence, the associated charge is = 0.001130529 VA / 0.15 Vs^{-1}

= **0.0075368 C**

Now, the number of electron transferred is = **0.0075368 C** / 1.602 $\times 10^{-19}$

= **0.0047046$\times 10^{19}$**

Since, the reduction of Co^{3+} to Co^{2+} is a single electron transfer reaction, the number electron calculated above is exactly the same as the number of surface-active sites.

Hence, the number of Co participate in OER is = **4.7046$\times 10^{16}$**

Calculated area associated with the reduction of Co^{3+} to Co^{2+} of CoFe-LDH/Cl^- = VA

Hence, the associated charge is = 0.00068998 VA/ 0.15 Vs^{-1}

= **0.004599 C**

Now, the number of electron transferred is = **0.004599 C**/ 1.602 $\times 10^{-19}$

= **0.002871$\times 10^{19}$**

Since, the reduction of Co^{3+} to Co^{2+} is a single electron transfer reaction, the number electron calculated above is exactly the same as the number of surface-active sites.

Hence, the number of Co participate in OER is = **2.871×10^{16}**

Calculated area associated with the reduction of Co^{3+} to Co^{2+} of CoFe-LDH/Bare = 0.0003179 VA

Hence, the associated charge is = 0.003179 VA/ 0.15 Vs^{-1}

= **0.00354 C**

Now, the number of electron transferred is = **0.002119 C**/ 1.602×10^{-19}

= **0.001322×10^{19}**

Since, the reduction of Co^{3+} to Co^{2+} is a single electron transfer reaction, the number electron calculated above is exactly the same as the number of surface-active sites.

Hence, the number of Co participate in OER is = **1.322×10^{16}**

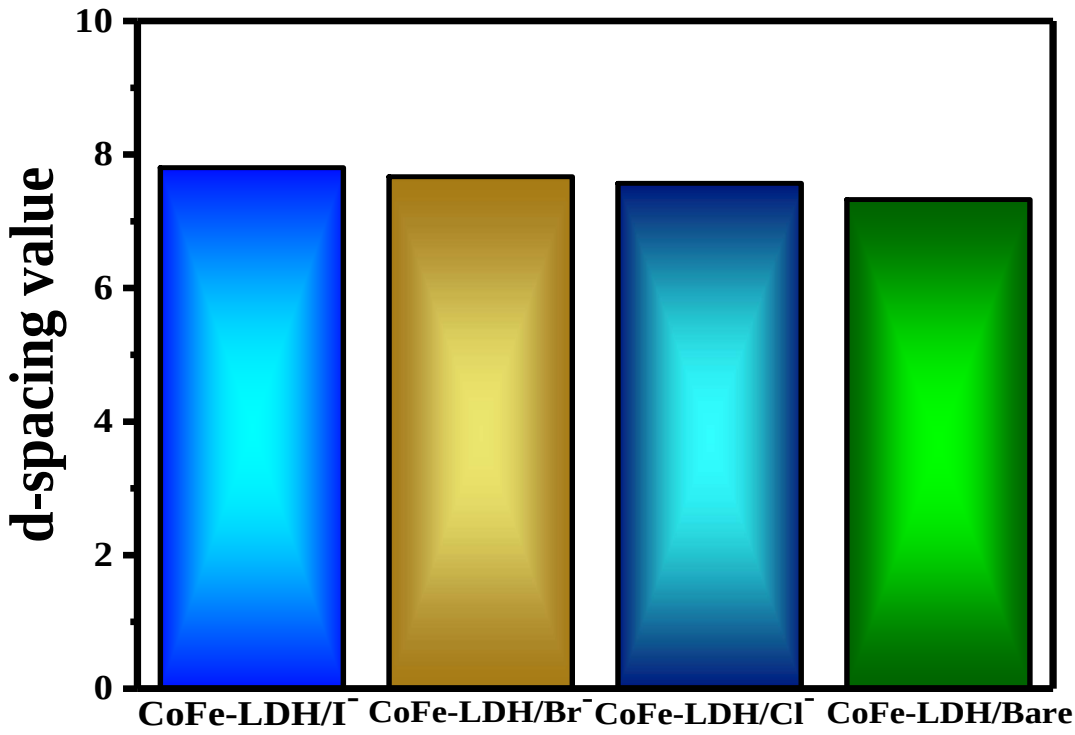

Figure S1: Calculated d-spacing values CoFe-LDH/I^- CoFe-LDH/Br^-, CoFe-LDH/Cl^- and CoFe-LDH/Bare.

Figure S1 The d-spacing values of all catalysts were calculated by using following formulae, $d = n\lambda /2dSin\theta$. The d space states that the distance between the two atomic planes. Hence here in this case the material without guest anion CoFe-LDH shows d-spacing value of 7.32 Å, whereas with guest anion it shows 7.56, 7.66 and 7.80 Å. Hence while intercalating the guest anions d-space value also increase which suggest that interlayer distance of LDHs increase gradually as per the size of the anions.

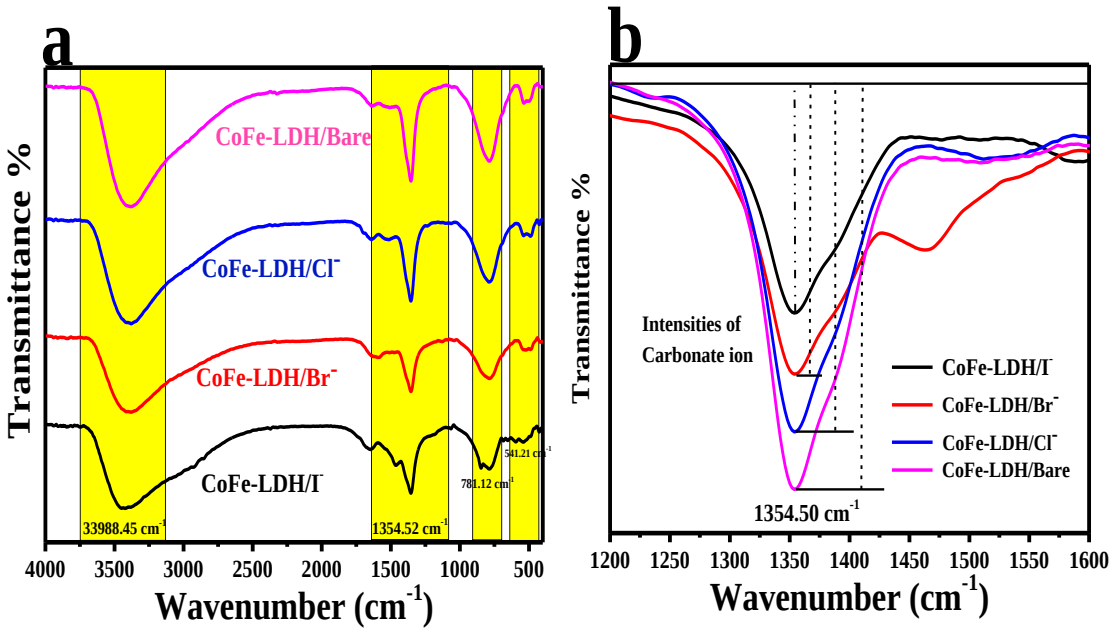

Figure S2. (a) FT-IR spectrum of CoFe-LDH/I^- CoFe-LDH/Br^-, CoFe-LDH/Cl^- and CoFe-LDH/Bare and (b) enlarged FT-IR spectrum of CoFe-LDH/I^- CoFe-LDH/Br^-, CoFe-LDH/Cl^- and CoFe-LDH/Bare.

Figure S2a is the FT-IR spectrum for all prepared catalyst, which is used to analyze the interlayer anions of prepared CoFe-LDHs material. Figure S2b is the enlarged FT-IR spectrum of all prepared CpoFe-LDHs materials.

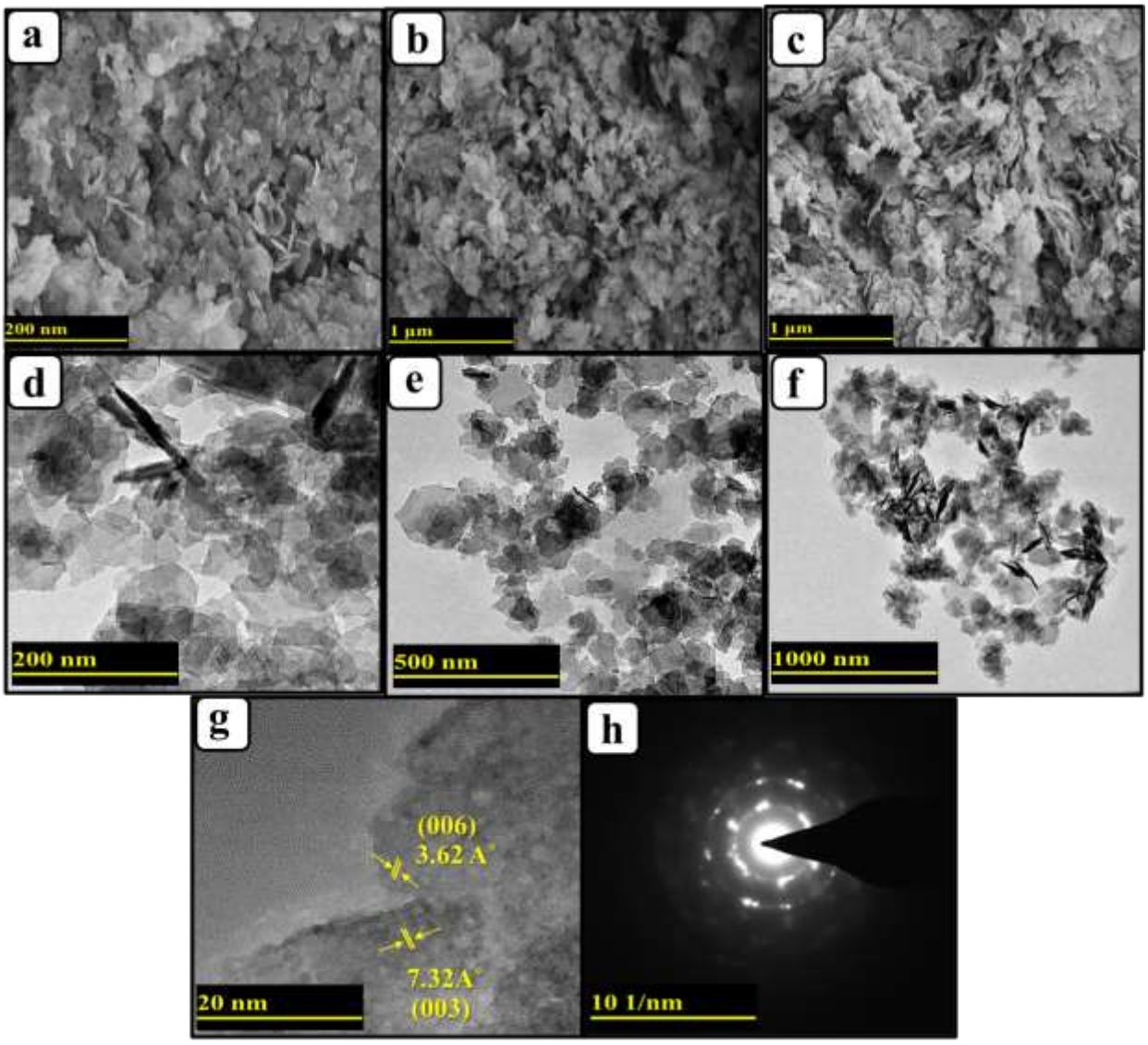

Figure S3. (a-c) High to Low magnification FE-SEM images of CoFe-LDH/Bare; (d-f) High to Low magnification HR-TEM images CoFe-LDH/Bare; (g) lattice fringes of CoFe-LDH/Bare and (h) SAED pattern of CoFe-LDH/Bare.

Figure S3 shows the microscopic images of CoFe-LDH/Bare. FE-SEM and TEM images from **Figure S3, [(a-c) and (d-f)]**, revels that materials are in hexagonal sheet like structure. HR-TEM images of **Figure S3g** shows the lattice fringes of CoFe-LDH/Bare with d-spacing values of 3.62 and 7.32 Å, are consistent with (006) and (003) plane. The SAED pattern of CoFe-LDH/Bare (**Figure S3h)** suggest that the material is in polycrystalline nature.

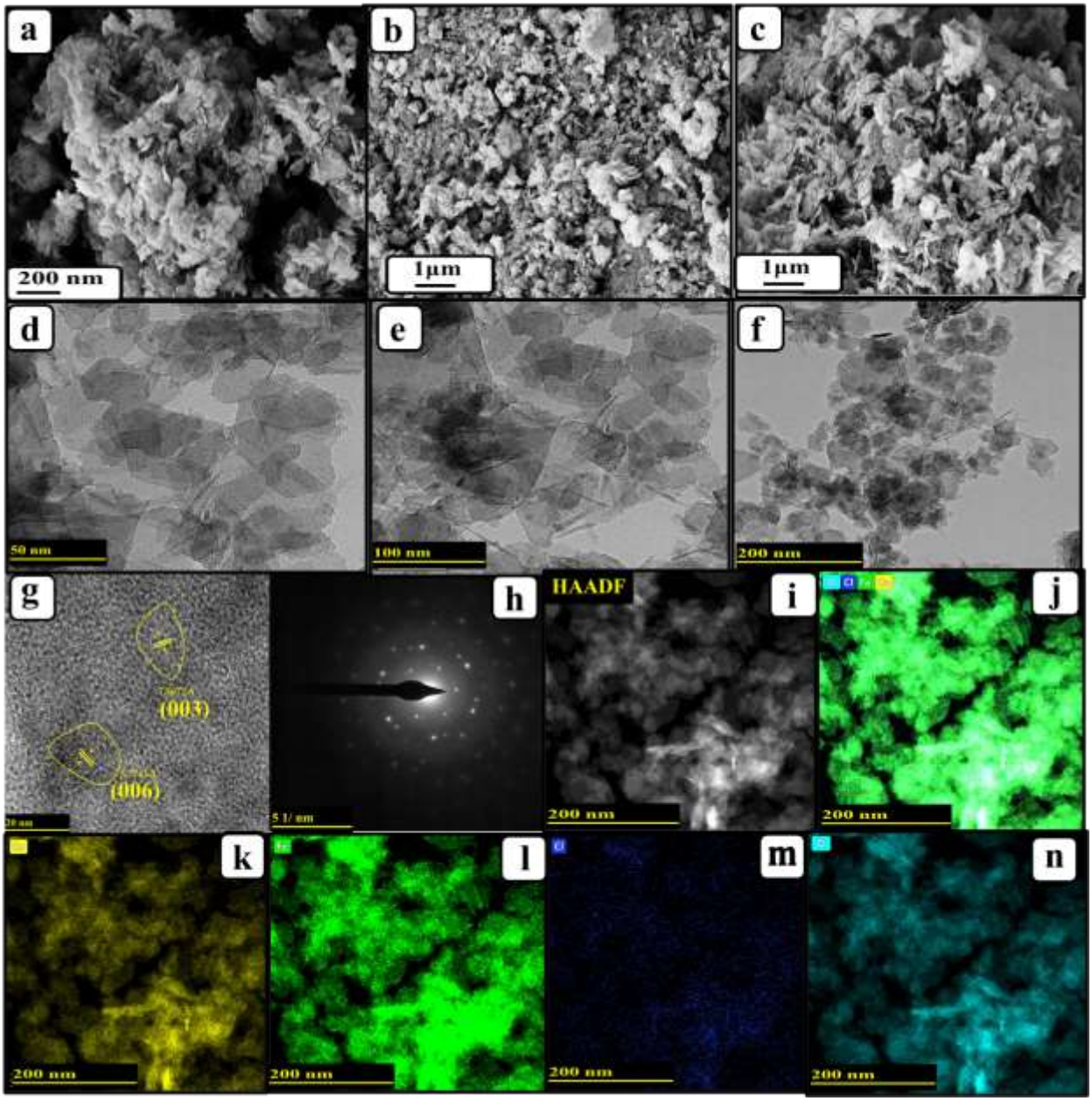

Figure S4. (a-c) High to Low magnification FE-SEM images of CoFe-LDH/Cl^{-}; (d-f) High to Low magnification HR-TEM images CoFe-LDH/Cl^{-}; (g) lattice fringes of CoFe-LDH/Cl^{-} and (h) SAED pattern of CoFe-LDH/Cl^{-}; (i) HAADF area chosen for colour mapping and (j-n) showing the colour mapping results of CoFe-LDH/Cl^{-} mix, Co, Fe, Cl^{-} and O respectively.

Figure S4 shows the microscopic images of CoFe-LDH/Cl^{-}. FE-SEM and TEM images from **Figure S4, [(a-c) and (d-f)]**, revels that materials are in hexagonal sheet like structure. HR-TEM images of **Figure S4g** shows the lattice fringes of CoFe-LDH/Cl^{-} with d-spacing values of 3.77

and 7.56 Å, are consistent with (006) and (003) plane. The SAED pattern of CoFe-LDH/Cl^- (**Figure S4h)** suggest that the material is in polycrystalline nature. **Figure S4i** shows the HR-TEM HAADF image of CoFe-LDH/Cl^- and the same was exposed to mapping analysis. Hence, **Figure S4[j-n]** demonstrates the uniform distribution of all respective elements (Co, Fe, O and Cl^-).

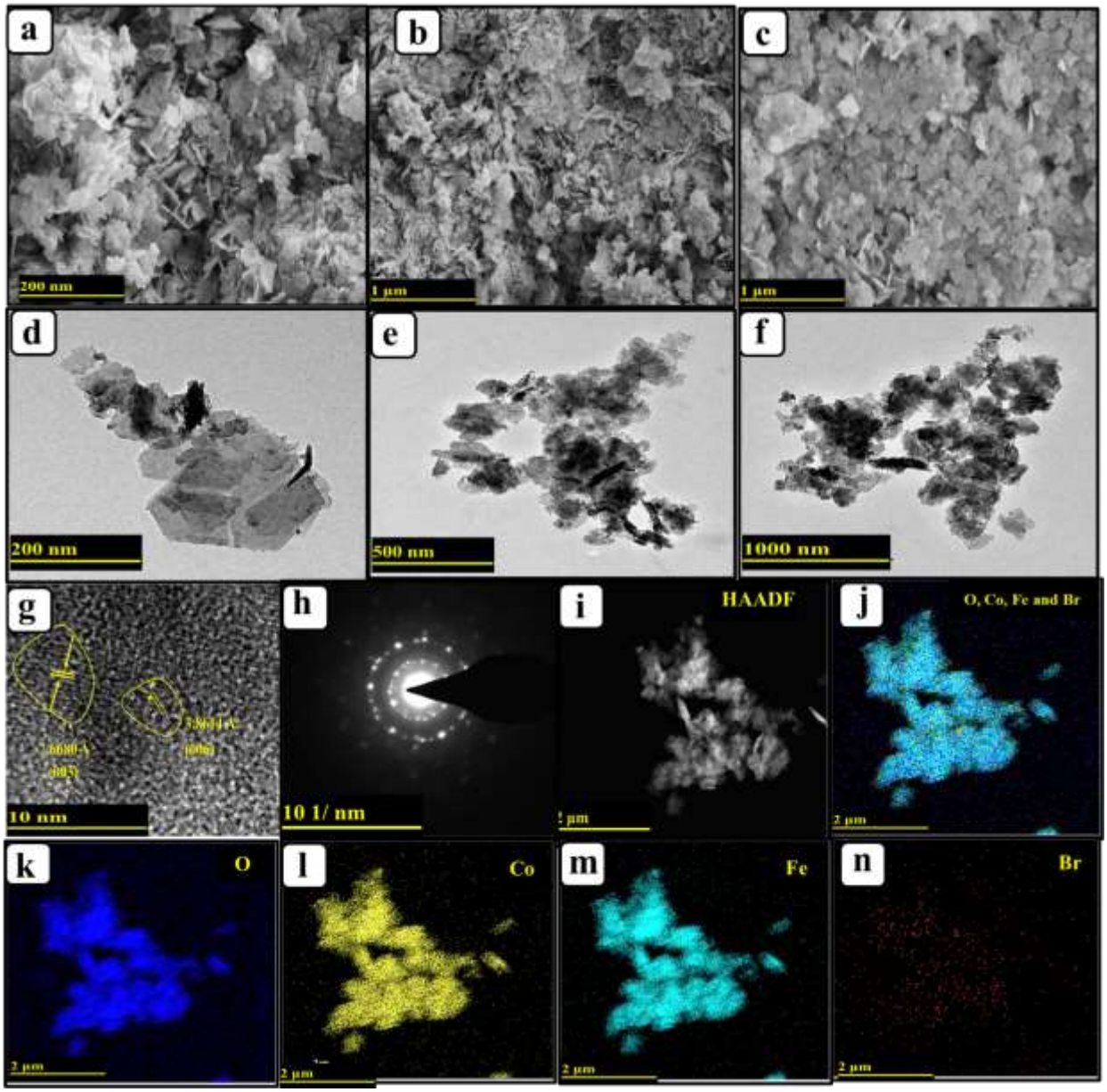

Figure S5. (a-c) High to Low magnification FE-SEM images of CoFe-LDH/Br^-; (d-f) High to Low magnification HR-TEM images CoFe-LDH/Br^-; (g) lattice fringes of CoFe-LDH/Br^- and (h) SAED pattern of CoFe-LDH/Br^-; (i) HAADF area chosen for colour mapping and (j-n) showing the colour mapping results of CoFe-LDH/Br^- mix, O, Co, Fe and Br^- respectively.

Figure S5 shows the microscopic images of CoFe-LDH/Br^-. FE-SEM and TEM images from **Figure S5, [(a-c) and (d-f)]**, revels that materials are in hexagonal sheet like structure. HR-TEM

images of **Figure S4g** shows the lattice fringes of CoFe-LDH/$Br^-$with d-spacing values of 3.86 and 7.66 Å, are consistent with (006) and (003) plane. The SAED pattern of CoFe-LDH/Br^-. (**Figure S4h)** suggest that the material is in polycrystalline nature. **Figure S4i** shows the HR-TEM HAADF image of CoFe-LDH/Br^- and the same was exposed to mapping analysis. Hence, **Figure S4[j-n]** demonstrates the uniform distribution of all respective elements (Co, Fe, O and Br^-).

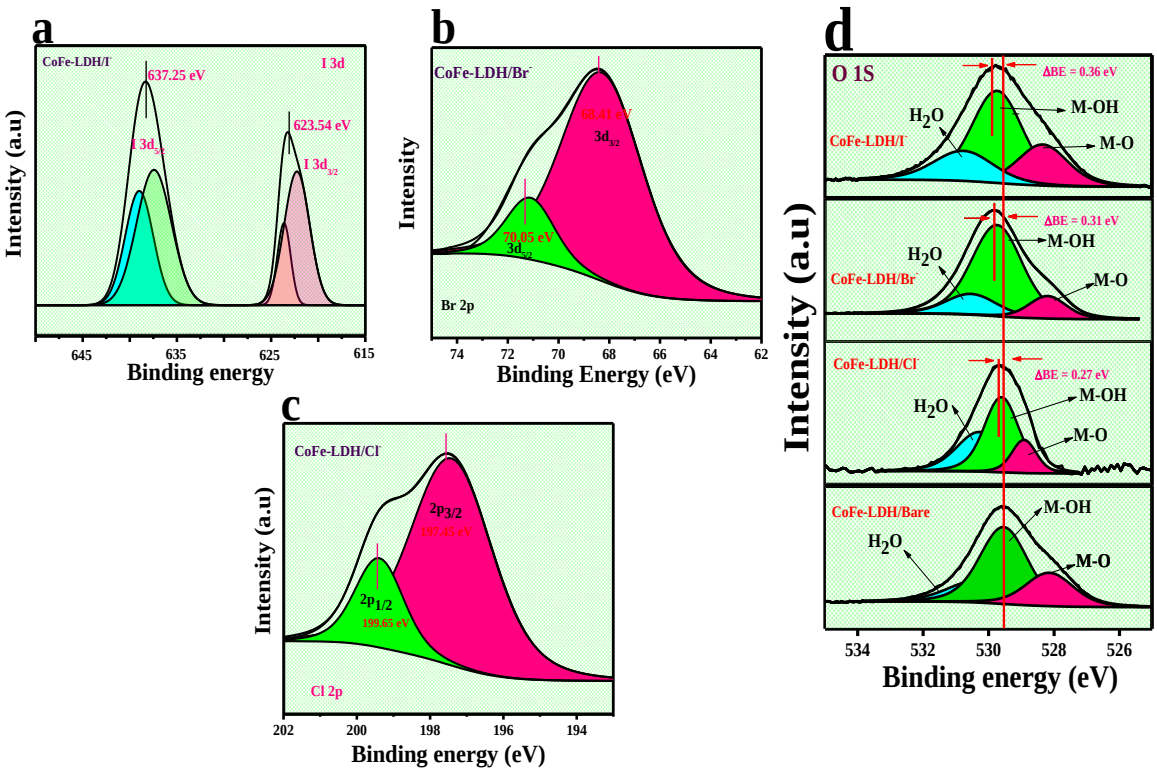

Figure S6. (a) Deconvoluted XPS spectrum of I 3d orbitals of CoFe-LDH/I^-; (b) deconvoluted XPS spectrum of Br 3d orbitals of CoFe-LDH/Br^-; (c) deconvoluted XPS spectrum of Cl 2p orbitals of $CoFe-LDH/Cl^-$ and (d) deconvoluted XPS spectrum of O 1s orbitals of CoFe-LDH/Bare, CoFe-LDH/Cl^-, CoFe-LDH/Br^- and CoFe-LDH/I^-.

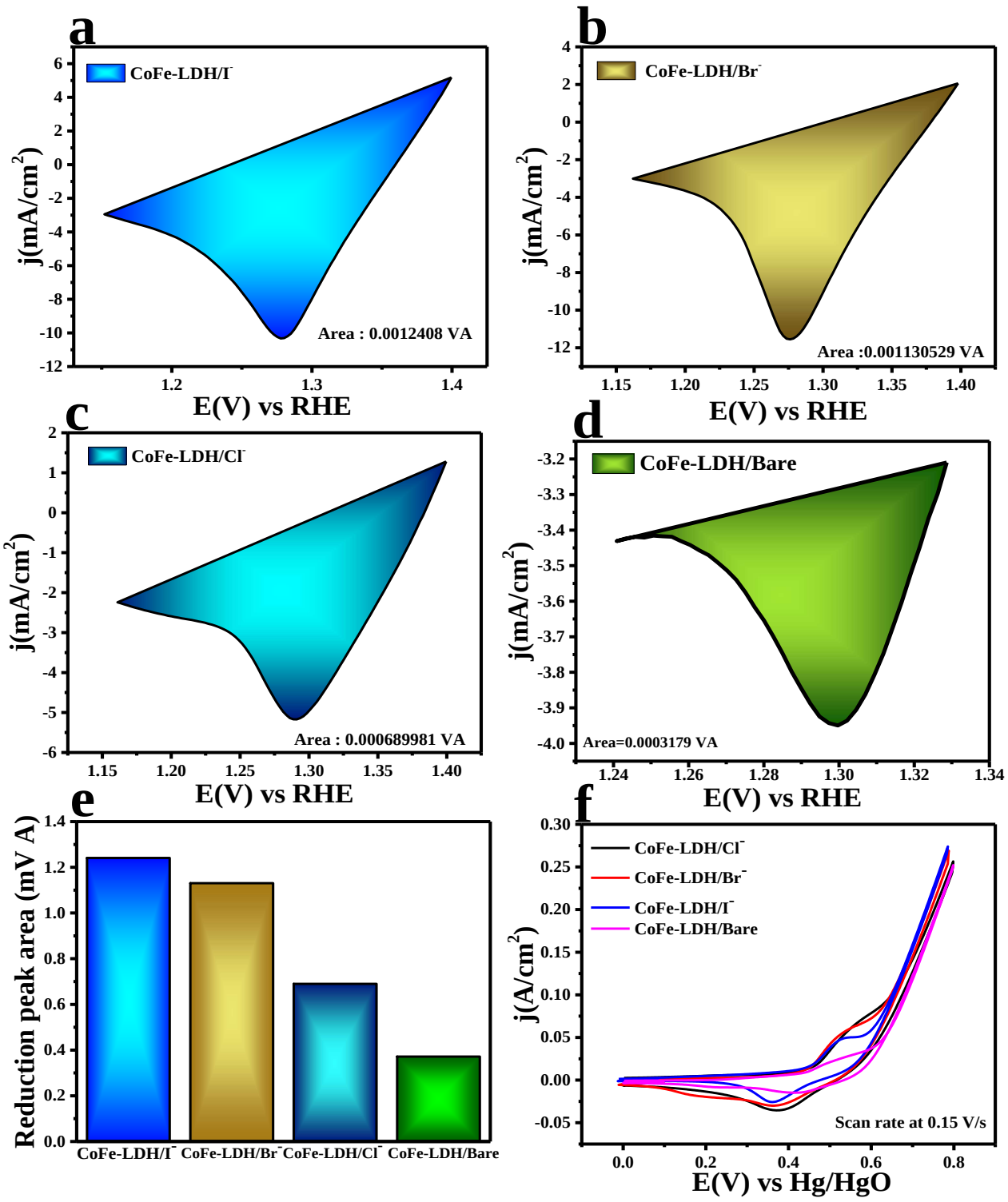

Figure S7. a-d) Reduction surface area for CoFe-LDH/I^{-} CoFe-LDH/Br^{-}, CoFe-LDH/Cl^{-} and CoFe-LDH/Bare; e) bar diagram for reduction surface area for CoFe-LDH/I^{-} CoFe-LDH/Br^{-}, CoFe-LDH/Cl^{-} and CoFe-LDH/Bare; f) CV cycle at 0.15 V/sec scan rate.

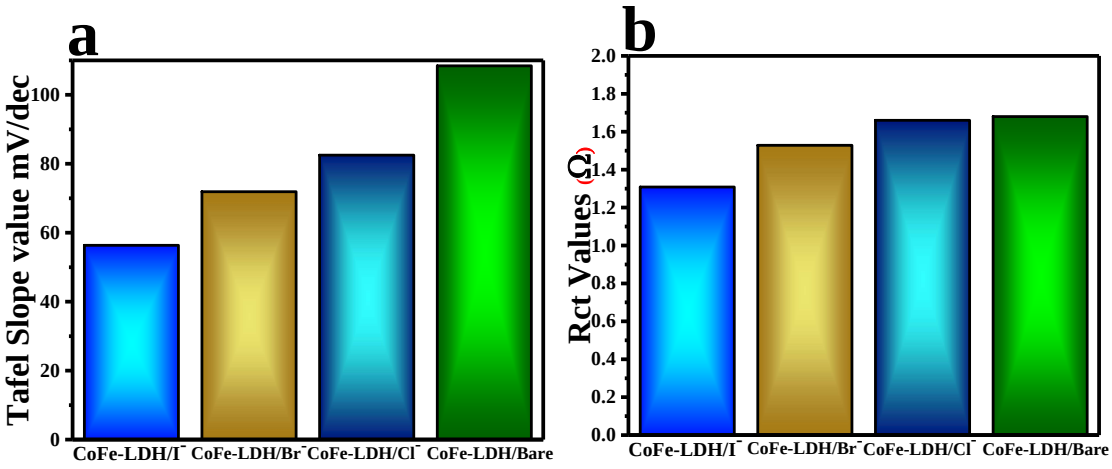

Figure S8. Bar diagram for the Tafel slope value (a) and R_{ct} value (b) for all prepared catalyst.

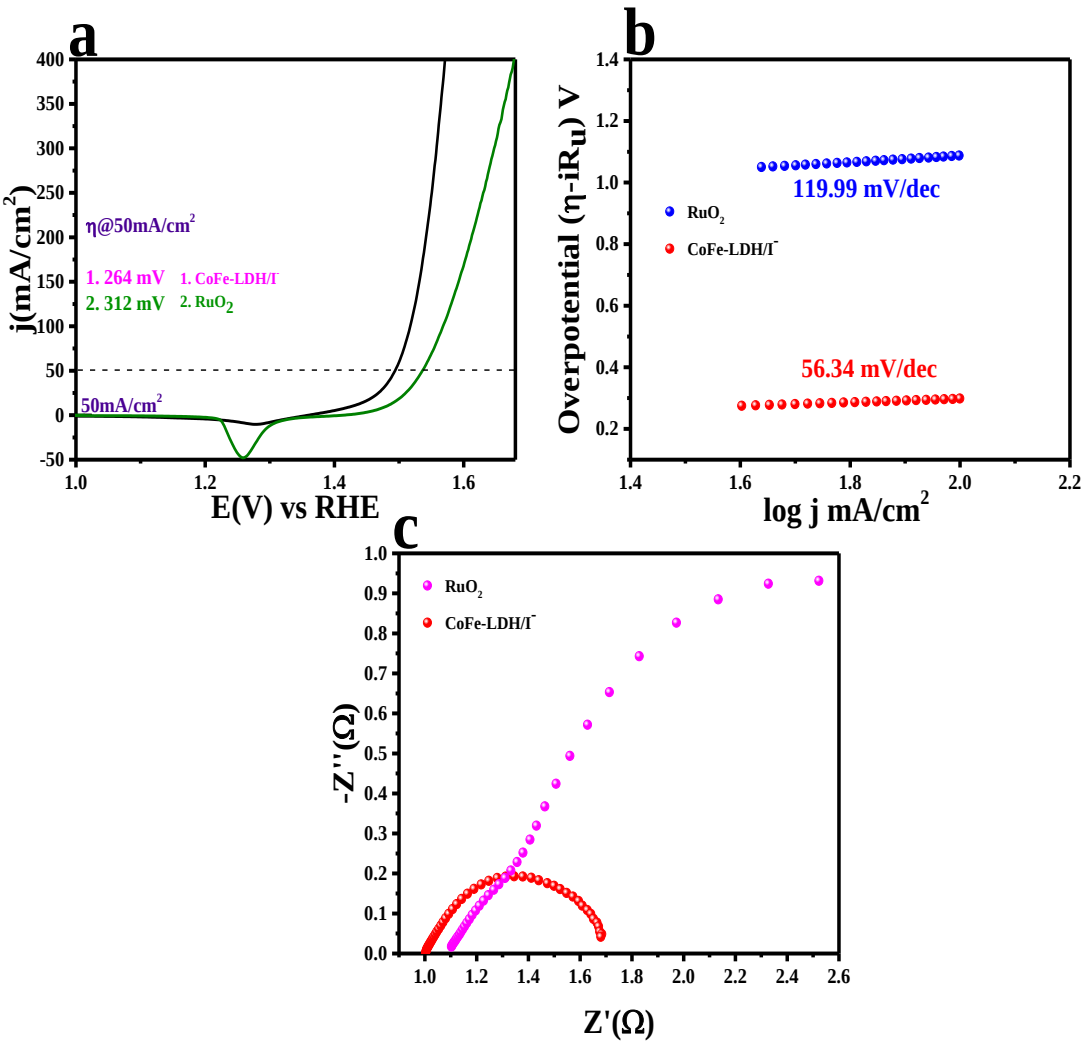

Figure S9. a) LSV curve; b) Tafel slope value; and c) Nyquist plot of RuO_2 and CoFe-LDH/I^-.

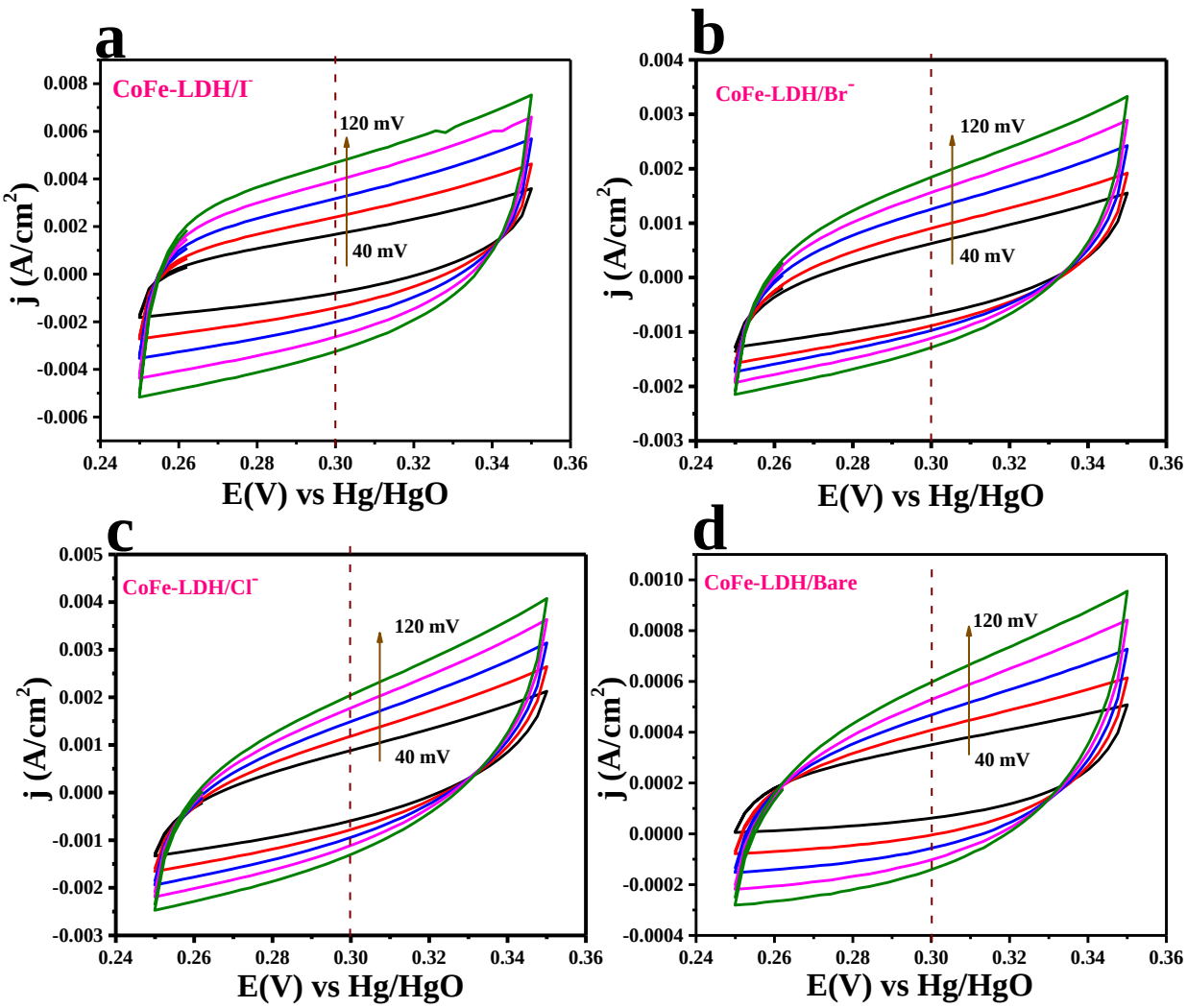

Figure S10. a-d) Scan rate dependent CV curves obtained for calculating the Cdl value in non-faradaic region of 0.25-0.35 V vs Hg/HgO for CoFe-LDH/I^-, CoFe-LDH/Br^-, CoFe-LDH/Cl^- and CoFe-LDH/Bare, respectively.

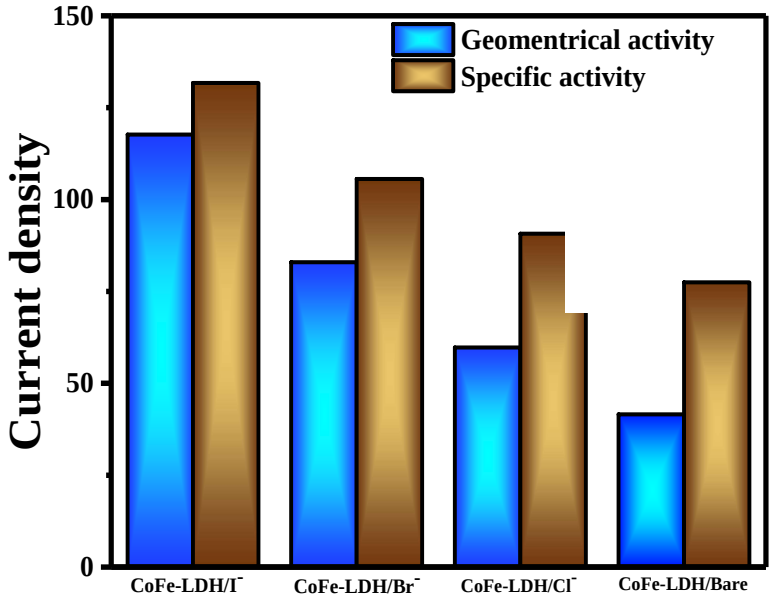

Figure S11. Bar diagram of geometrical and specific activity profile.

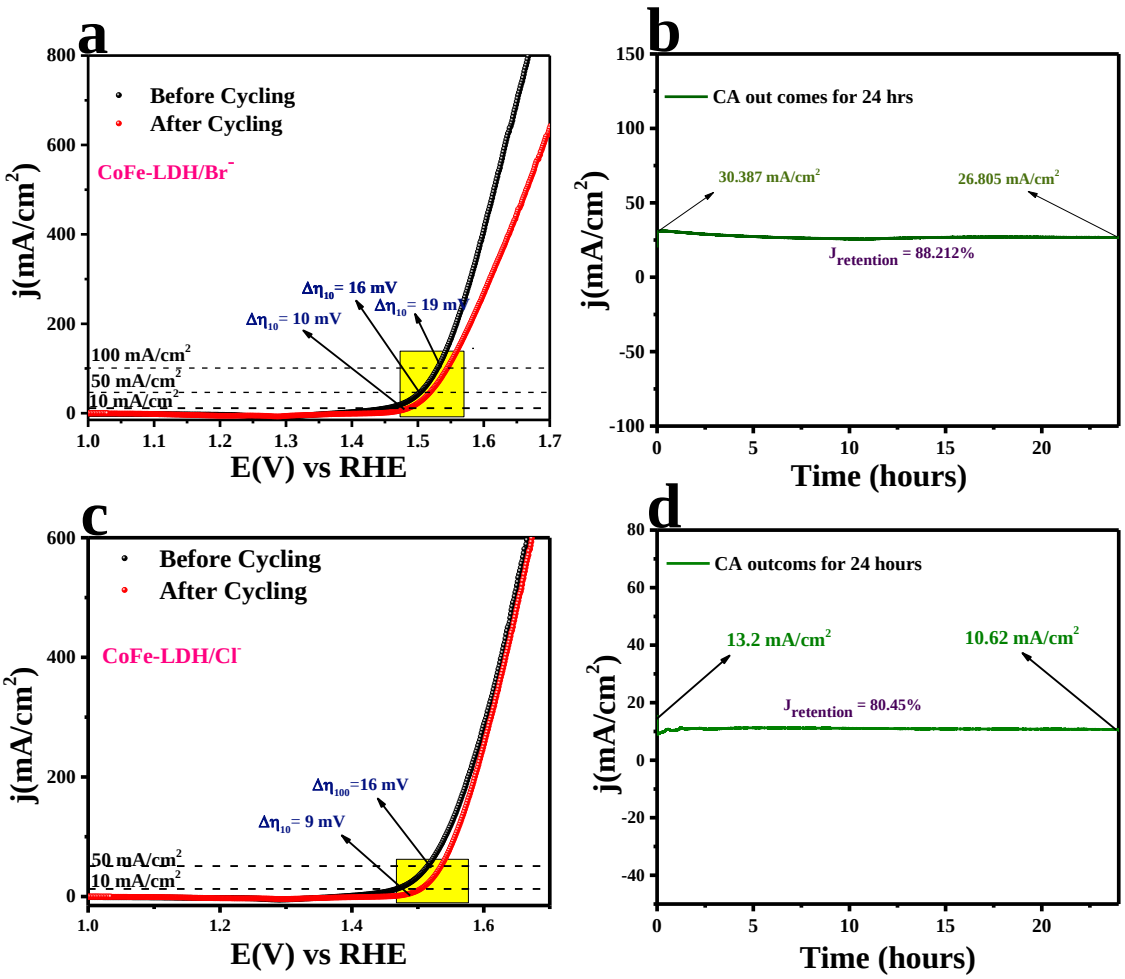

Figure S12. a) LSV polarization outcomes after and before 1500 number of cycling for CoFe-LDH/Br^-; b) chronoamperometric outcomes of CoFe-LDH/Br^-; c) LSV polarization outcomes after and before 1500 number of cycling for CoFe-LDH/Cl^- and d) chronoamperometric outcomes of CoFe-LDH/Cl^-.

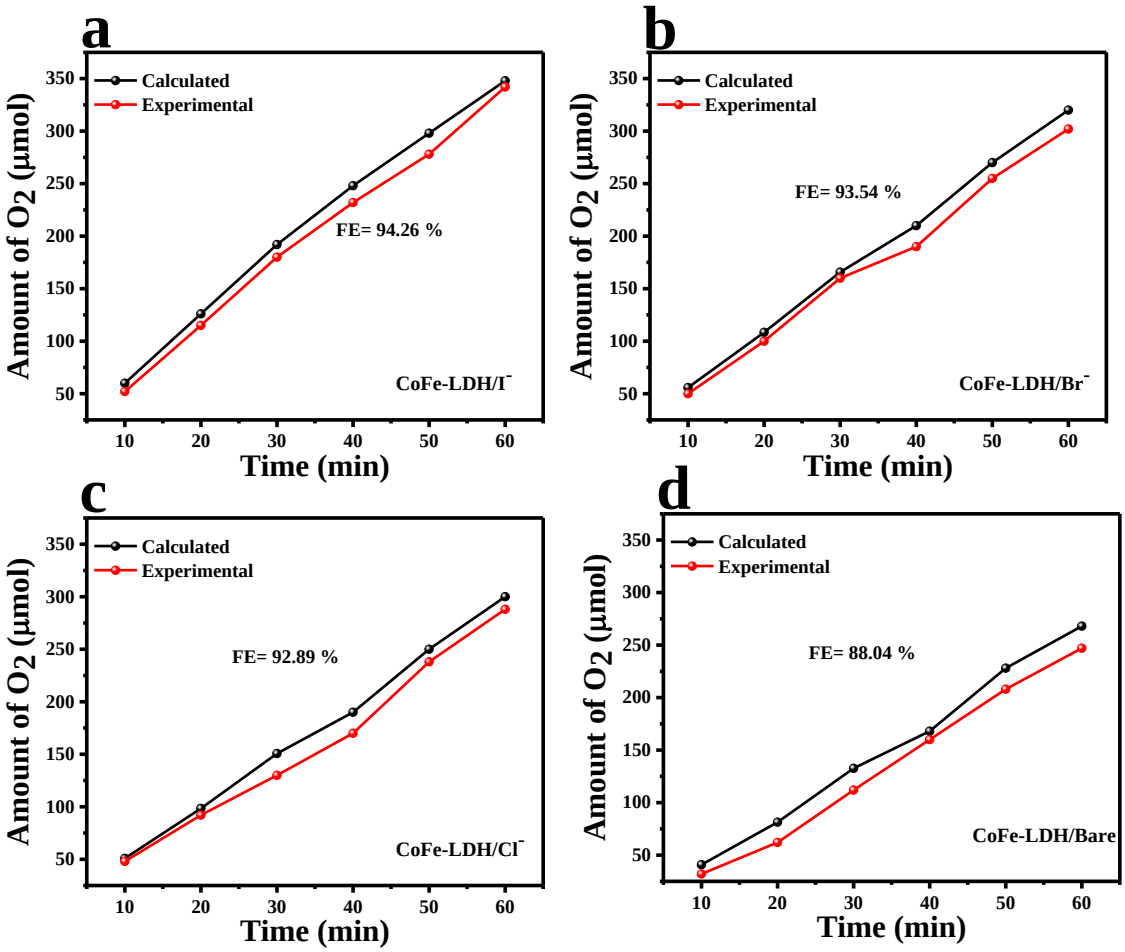

Figure S13. Faradaic efficiency plot for a) CoFe-LDH/I^-; b) CoFe-LDH/Br^-; c) CoFe-LDH/Cl^- and d) CoFe-LDH/Bare with a comparison experimentally produced and calculated amount of gas.

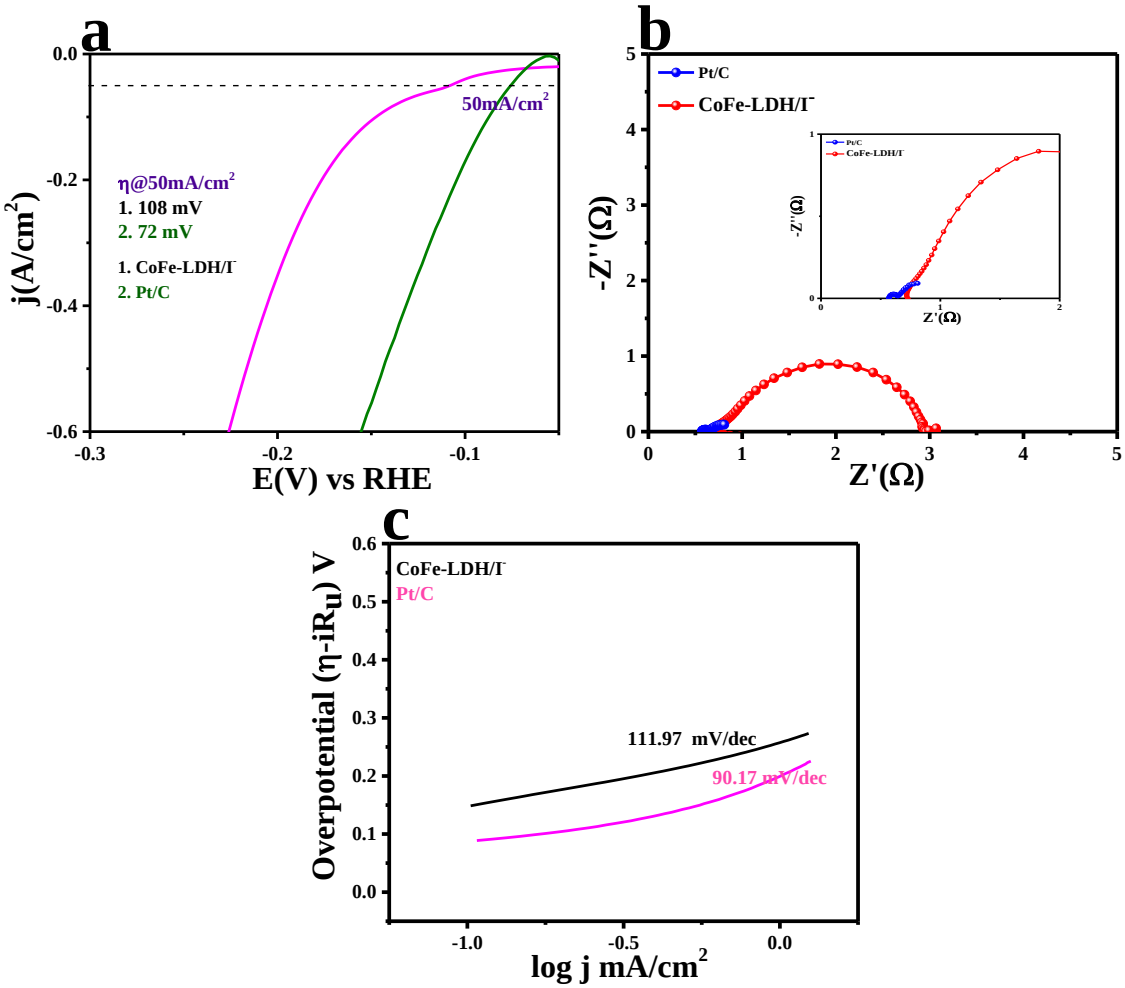

Figure S14. a) LSV curve; b) Tafel slope value; and c) Nyquist plot of Pt/C and CoFe-LDH/I^-.

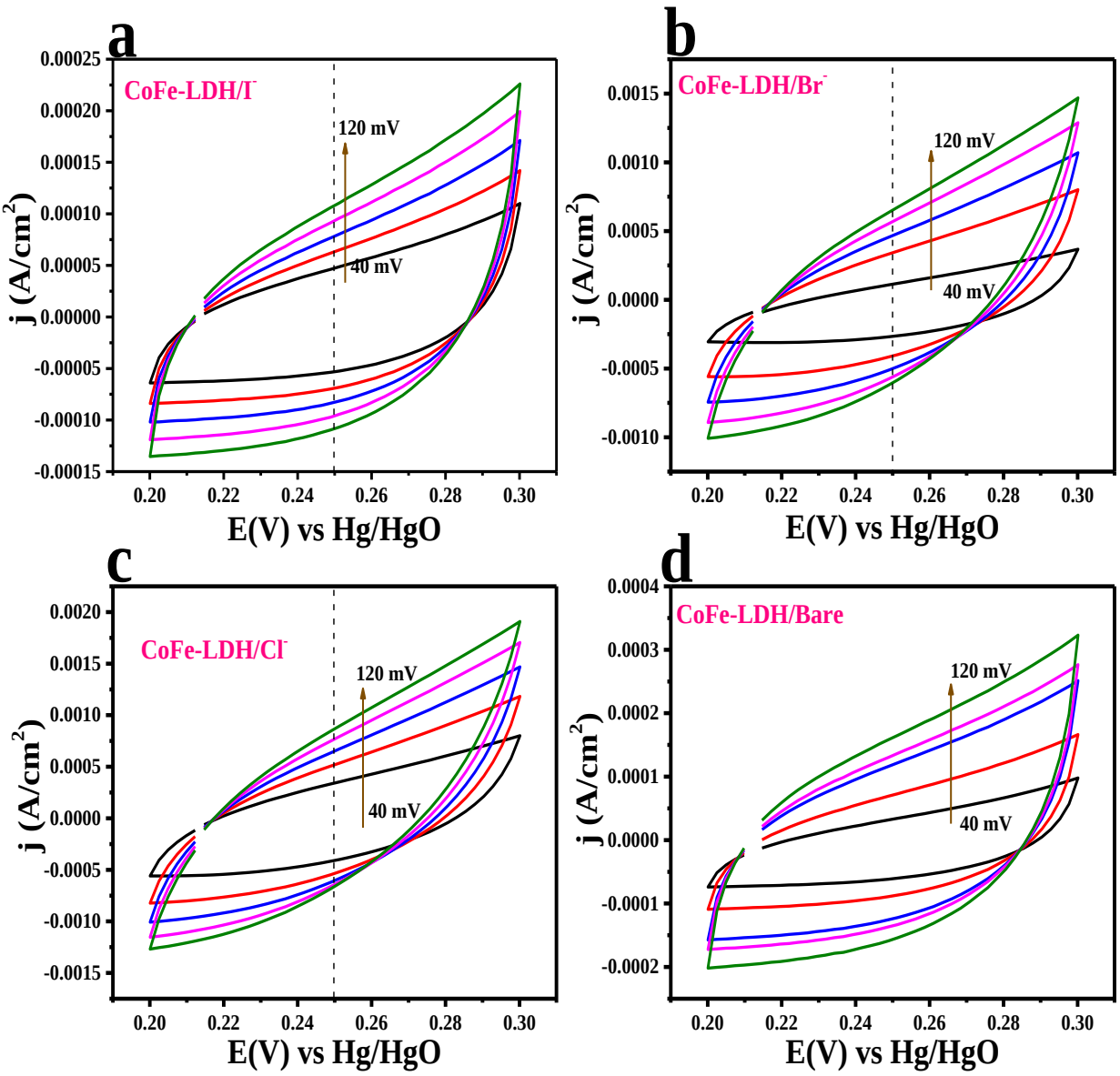

Figure S15. a-d) Scan rate dependent CV curves obtained for calculating the Cdl value in non-faradaic region of 0.25-0.35 V vs Hg/HgO for CoFe-LDH/I^-, CoFe-LDH/Br^-, CoFe-LDH/Cl^- and CoFe-LDH/Bare, respectively.

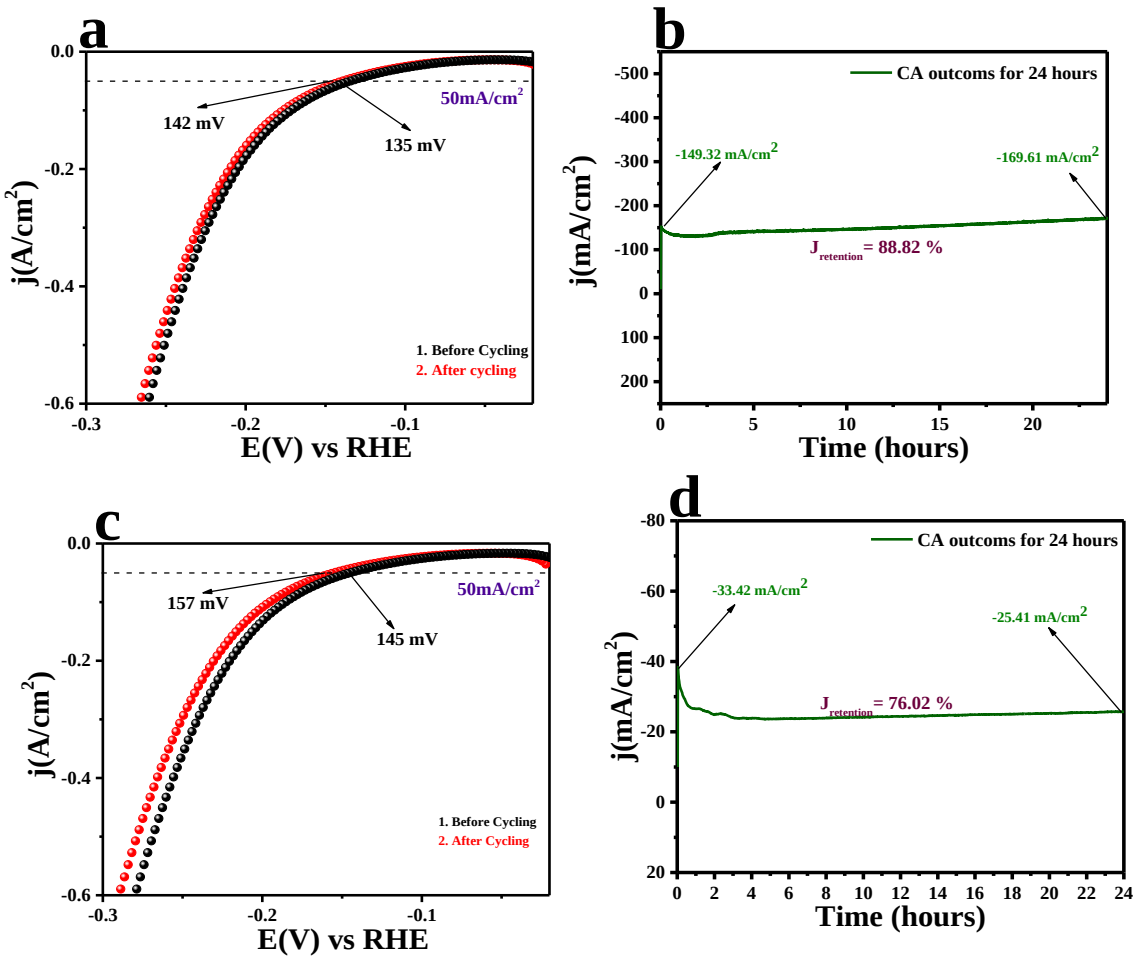

Figure S16. a) LSV polarization outcomes after and before 500 number of cycling for CoFe-LDH/Br^-; b) chronoamperometric outcomes of CoFe-LDH/Br^-; c) LSV polarization outcomes after and before 500 number of cycling for CoFe-LDH/Cl^- and d) chronoamperometric outcomes of CoFe-LDH/Cl^-.

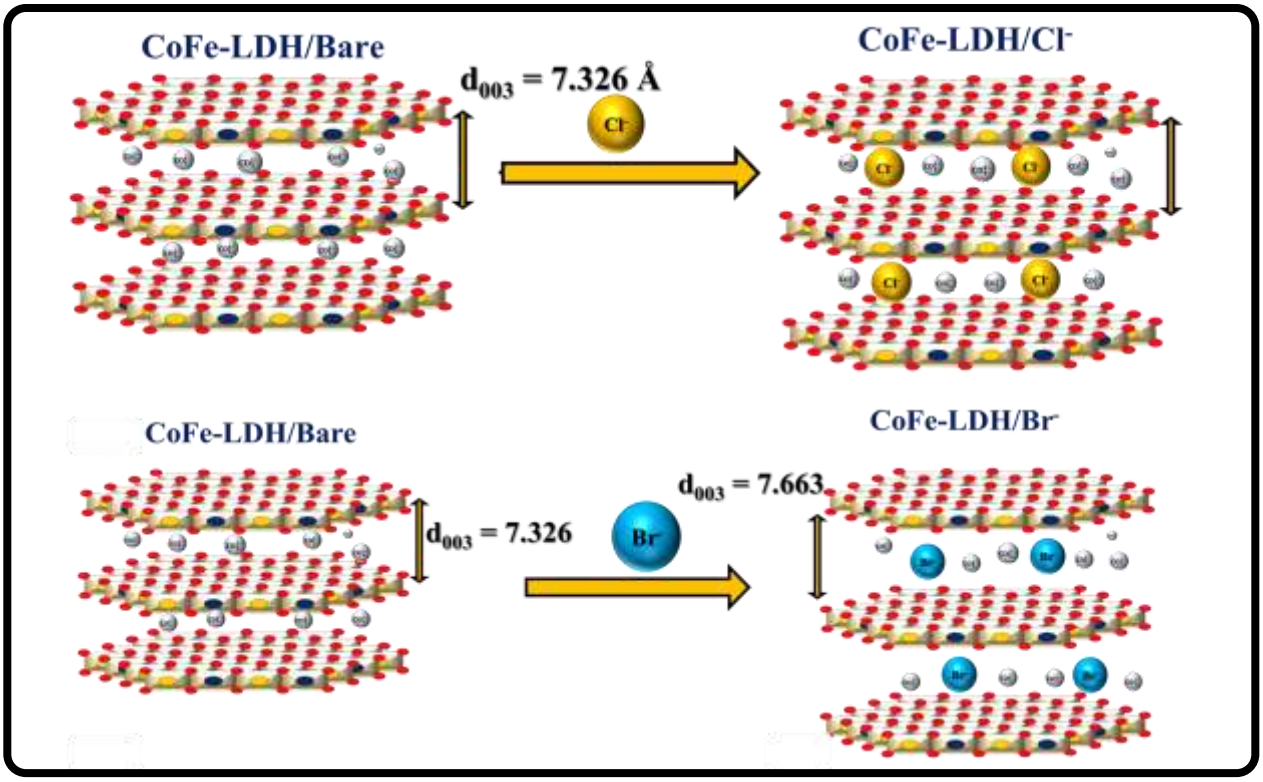

Figure S17. Schematic representation Intercalation of Guest Anions (Cl^-, Br^-) into CoFe-LDHs.

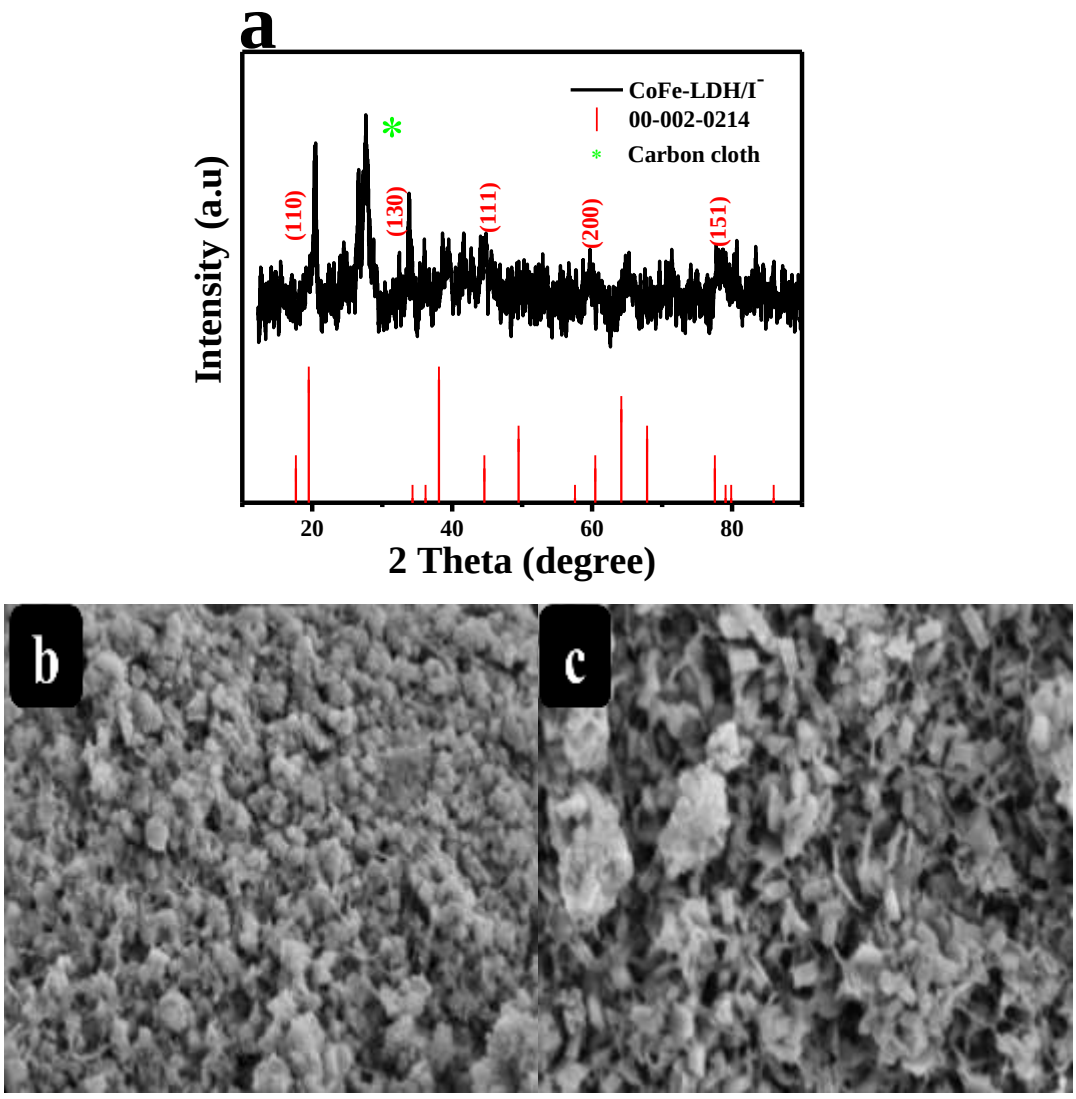

Figure S18. a) Post-XRD patterns of CoFe-LDH/I^-; b-c) low to high magnification Post-FE-SEM images of CoFe-LDH/I^-.

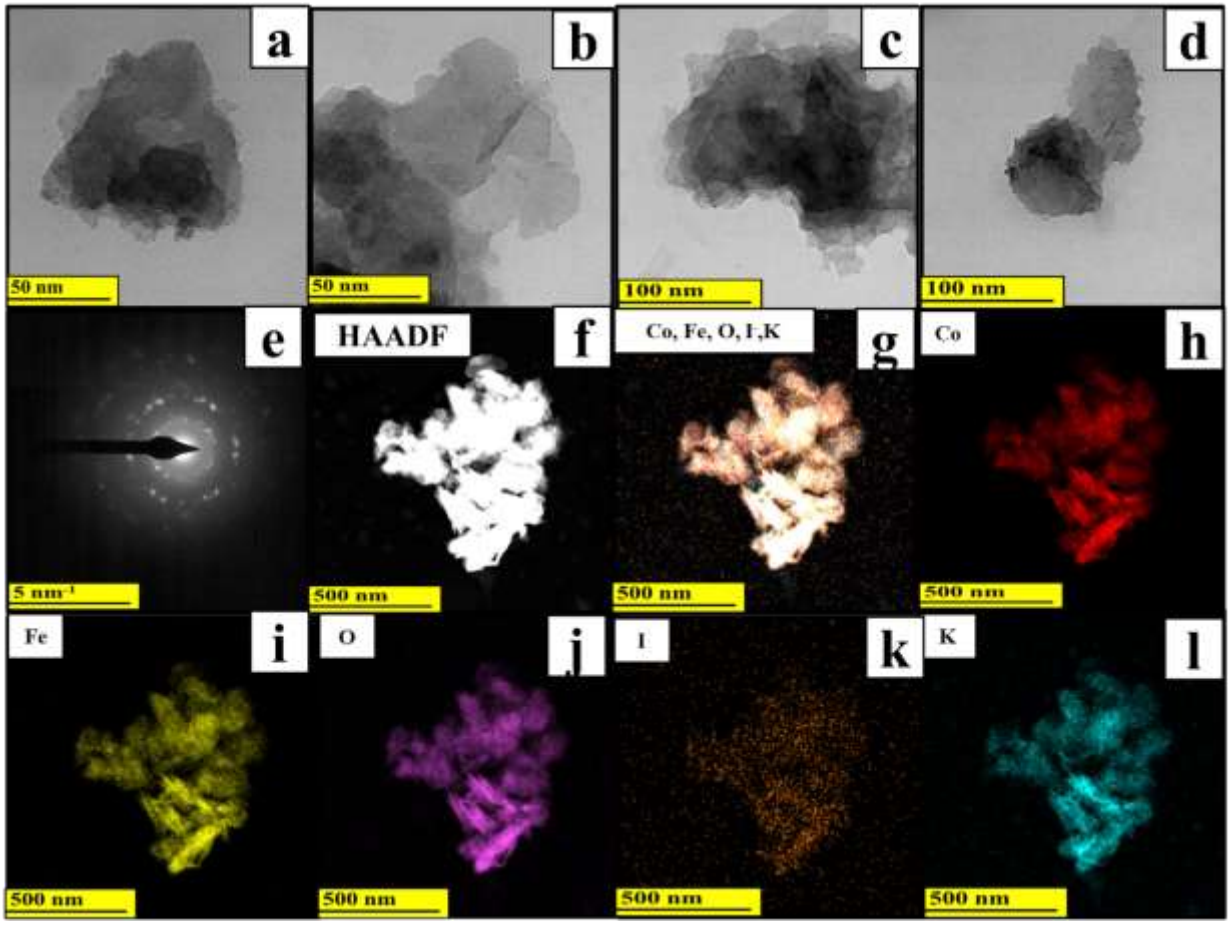

Figure S19. (a-d) High to Low magnification HR-TEM images post CoFe-LDH/I^-; (e) SAED pattern of Post CoFe-LDH/I^-; (f) HAADF area chosen for colour mapping and (g-l) Showing the colour mapping results of Post CoFe-LDH/I^- mix, O, Co, Fe, I and K respectively.

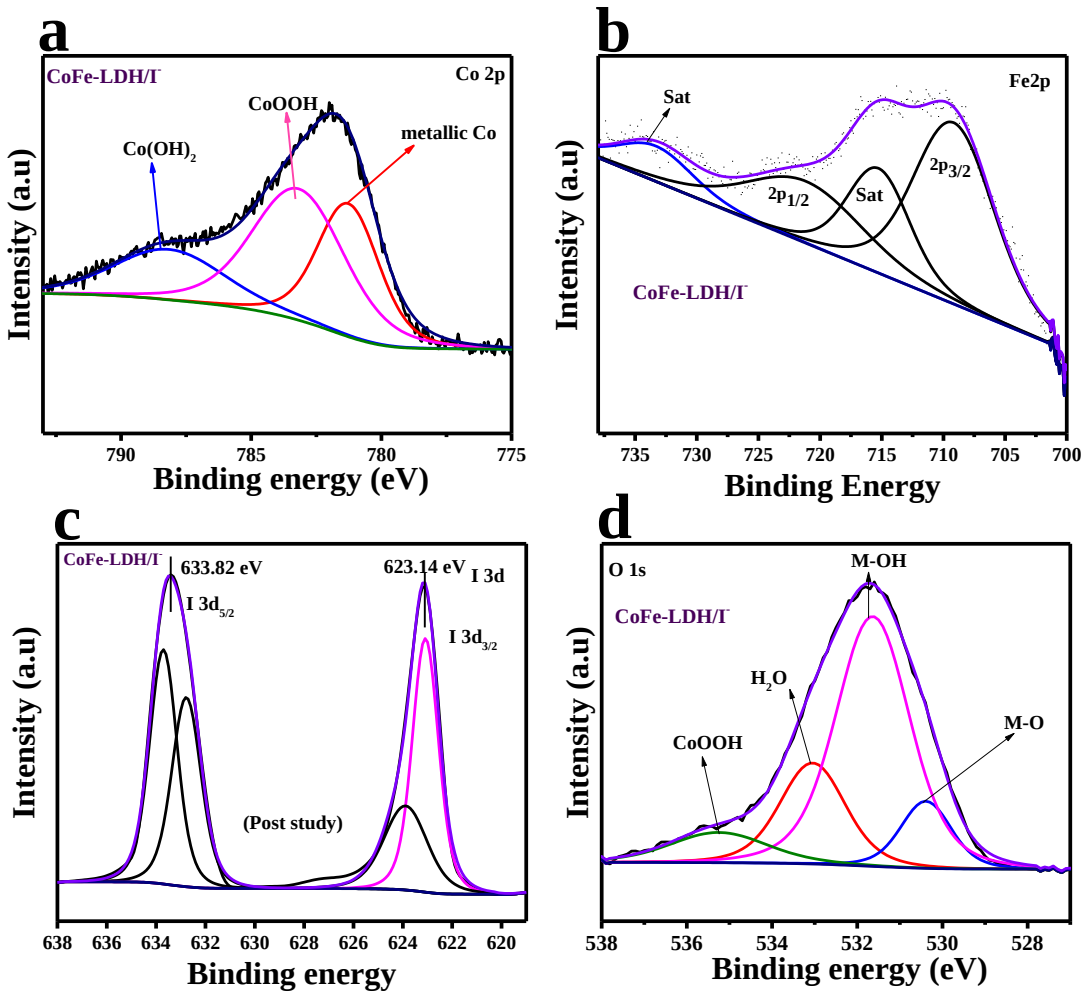

Figure S20. a) Deconvoluted post-XPS spectrum of Co 2p orbitals CoFe-LDH/I^-; b) deconvoluted post-XPS spectrum of Fe 2p orbitals CoFe-LDH/I^-; c) deconvoluted post-XPS spectrum of I 3d orbitals of CoFe-LDH/$I^-$and d) deconvoluted post-XPS spectrum of O 1s orbitals of CoFe-LDH/I^-

Catalyst	Cobalt	Iron	Host ions	Guest ions
CoFe-LDH/Br^-	0.1 M	0.1 M	0.4 M	0.1 M
CoFe-LDH/Cl^-	0.1 M	0.1 M	0.4 M	0.1 M
CoFe-LDH/I^-	0.1 M	0.1 M	0.4 M	0.1 M
CoFe-LDH/Bare	0.1 M	0.1 M	0.5 M	-

Table S1. Synthesized catalysts with different molar concentrations of CoFe-LDH.

Catalyst	ECSA for OER	ECSA for HER
CoFe-LDH/Bare	0.1465	0.185
CoFe-LDH/Cl^-	0.6135	0.524
CoFe-LDH/Br^-	0.7975	0.638
CoFe-LDH/I^-	0.90125	0.826

Table S2. ECSA values of all prepared catalyst.

Catalyst	Co^{3+}/Co^{2+}
CoFe-LDH/Cl^-	1.45
CoFe-LDH/Br^-	2.01
CoFe-LDH/I^-	3.23
CoFe-LDH/Bare	0.99

Table S3. The Co^{3+} to Co^{2+} ratio (Co^{2+}/Co^{3+}) of prepared catalyst, as derived from peak deconvolution of Co 2p core-level XPS spectra.

References:

1 S. Anantharaj, S. R. Ede, K. Sakthikumar, K. Karthick, S. Mishra and S. Kundu, *ACS Catal.*, 2016, **6**, 8069–8097.

2 R. Yang, Y. Zhou, Y. Xing, D. Li, D. Jiang, M. Chen, W. Shi and S. Yuan, *Appl. Catal. B Environ.*, 2019, **253**, 131–139.

3 W. Ma, R. Ma, J. Wu, P. Sun, X. Liu, K. Zhou and T. Sasaki, *Nanoscale*, 2016, **8**, 10425–10432.

4 A. Karmakar, K. Karthick, S. S. Sankar, S. Kumaravel, R. Madhu and S. Kundu, *J. Mater. Chem. A*, 2021, **9**, 1314–1352.

5 B. M. Hunter, W. Hieringer, J. R. Winkler, H. B. Gray and A. M. Müller, *Energy Environ. Sci.*, 2016, **9**, 1734–1743.

6 X. Yang, C.-J. Wang, C.-C. Hou, W.-F. Fu and Y. Chen, *ACS Sustain. Chem. Eng.*, 2018, **6**, 2893–2897.

7 M. W. Louie and A. T. Bell, *J. Am. Chem. Soc.*, 2013, **135**, 12329–12337.

8 A. I. Khan and D. O'Hare, *J. Mater. Chem.*, 2002, **12**, 3191–3198.

9 A. Schutz and P. Biloen, *J. Solid State Chem.*, 1987, **68**, 360–368.

10 S. A. Chala, M.-C. Tsai, B. W. Olbasa, K. Lakshmanan, W.-H. Huang, W.-N. Su, Y.-F. Liao, J.-F. Lee, H. Dai and B. J. Hwang, *ACS Nano*, 2021, **15**, 14996–15006.